Self-Collimation in Planar Photonic Crystals

Jeremy Witzens, Marko Lončar, and Axel Scherer

***Abstract*—We analyze, in three dimensions, the dispersion properties of dielectric slabs perforated with two-dimensional photonic crystals (PCs) of square symmetry. The band diagrams are calculated for *all* k-vectors in the first Brillouin zone, and not only along the characteristic high-symmetry directions. We have analyzed the equal-frequency contours of the first two bands, and we found that the square lattice planar photonic crystal is a good candidate for the self-collimation of light beams. We map out the group velocities for the second band of a square lattice planar PC and show that the group velocity is the highest in the region of maximum self-collimation. Such a self-collimated beam is predicted to show beating patterns due to the specific shape of the equal-frequency contours. A geometrical transformation maps the region of the first and second photonic bands where self-collimation takes place one onto the other and gives additional insights on the structural similarities of self-collimation in those two bands.**

***Index Terms*—Autocollimation, finite difference time domain (FDTD), planar photonic crystals, self-collimation.**

I. Introduction

In recent years, photonic crystals [1] (PCs) have attracted a lot of attention due to their ability to control the flow of light on a very small length scale. One class of PCs, planar photonic crystals [2] (PPCs), represent particularly promising structures for integrated optics due to the fact that their planar fabrication allows the use of conventional microelectronics patterning techniques. A PPC is an optically thin dielectric slab perforated with a two-dimensional (2-D) lattice of holes. Light is confined in the slab in the vertical direction by means of total internal reflection and in the lateral direction by distributed Bragg reflection, due to the presence of the 2-D lattice of holes [3], [4]. Most of the initial research done on PPC structures was focused on the use of the photonic bandgap (PBG) of the PC devices, in order to trap light. It was shown that by creating different types of defects in the PPC it is possible to make lasers [5] and waveguides [6], as well as coupled photonic devices [7], [8].

On the other hand, there has been a growing interest in the very interesting dispersion characteristics of PCs [9], [10]. Phenomena like superprism [11] and self-collimation [12] have already been observed in the case of a three-dimensional (3-D) "autocloned" PC structure [13]. Recently, there has been an effort to implement those phenomena in PPCs [14]–[17]. Those are important results since the fabrication of PPCs [6] allows an easy integration of different devices on a single chip. The superprism effect has been investigated theoretically and experimentally in PPCs [16], [17] and a paper by Notomi [14] explores the conceptual framework to understand dispersion in PCs. In this paper we investigate self-collimation in PPCs and show novel effects such as beating patterns, as well as the possibility to transfer a self-collimated beam between two types of PCs with low distortion and low losses.

Manuscript received September 3, 2002; revised September 30, 2002. This work was supported in part by DARPA under Contract MDA972–00-1–0022 and Contract MDA972–00-1–0019, as well as the Air Force Office of Scientific Research under Contract F49620–01-1–0497.

The authors are with the Department of Electrical Engineering, California Institute of Technology, Pasadena, CA 91125 USA (e-mail: witzens@caltech.edu).

Digital Object Identifier 10.1109/JSTQE.2002.806693

II. 3-D Finite Difference Time-Domain Analysis of Self-Collimation in a Square Lattice PPC

The structure that we are considering here is a silicon slab (refractive index $n_{\mathrm{Si}} = 3.5$) of thickness $t = 0.57a$ and patterned with a two-dimensional (2-D) square lattice of holes of radius $r = 0.3a$, where a is the periodicity of the lattice. The slab is surrounded by air on both sides. We have used a three-dimensional (3-D) finite difference time-domain (3-D FDTD) code [18] to analyze one unit cell of the structure by applying appropriate boundary conditions to the sides of the computational domain, as indicated in the Fig. 1(a). The discretization used in our 3-D FDTD algorithm was 30 computation points per lattice period a. We have analyzed only one half of the structure in the vertical direction by applying the mirror boundary condition at the center of the slab (slab half thickness was $t/2 = 8$ computational points). By choosing the type of mirror symmetry (even or odd), we could select between TE-like (vertically even) or TM-like (vertically odd) eigenmodes of the PPC. Mur's absorbing boundary conditions [18] were applied at 100 computational points away from the surface of the slab, yielding a computational domain of $30 \cdot 30 \cdot 108$ cubic cells. More details on the band diagram analysis of PPCs using the FDTD method can be found in previous publications [6].

The starting point for the investigation of any PPC-based device is the calculation of a dispersion diagram for the modes supported in the PPC. In Fig. 1(b) we show such a band diagram for the case of a square lattice PPC, obtained by using 3-D FDTD. The band diagram is calculated only along the high-symmetry directions in the first Brillouin zone (I BZ), and the light cone is represented by the gray region. Only the modes that lie outside the light cone (i.e., below the light line) are guided in the PPC by total internal reflection, i.e., without any losses other than absorption, scattering, and imperfect lithography. In other words, only modes outside the light cone are lossless in the ideal PPC. We can see that this structure has a small bandgap. However, the width of the bandgap is not what concerns us here. We instead hope to find unusual phenomena associated with the difference between the dispersion diagram of this structure and the dispersion diagram of an unpatterned slab. In order to do so, we have to calculate the *full* band diagram for *all* k- vectors in the I BZ, and not only along ΓX, XM, and ΓM directions [15].

Fig. 2(a) shows such a dispersion diagram for the first two bands [black circles in the Fig. 1(b)] for *all* k-vectors in the I

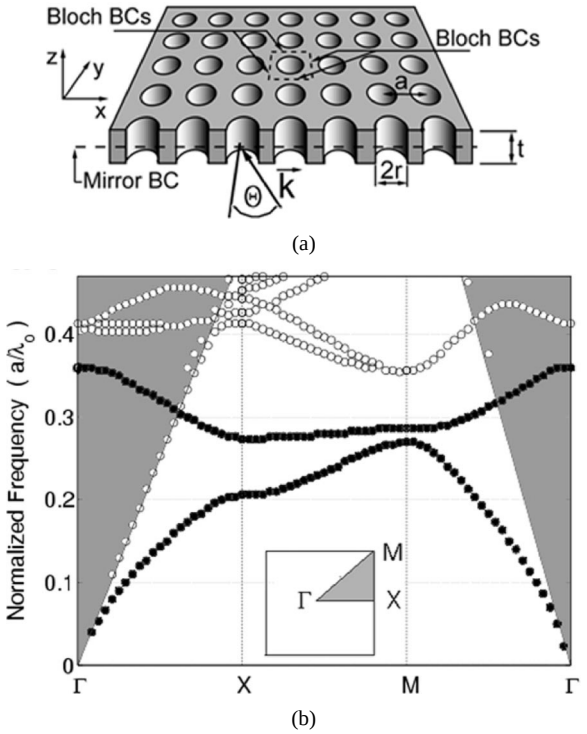

Fig. 1. (a) Schematic view of the Si slab patterned with a 2-D square lattice of holes. External light is incident on the slab at an angle θ. Unit cell of the PC, with boundary conditions used in the 3-D FDTD calculation, is also indicated. (b) Band diagram for TE-like (vertically even) modes of the square lattice PPC. The gray region represents the light cone. Inset shows high-symmetry points in the first Brillouin zone.

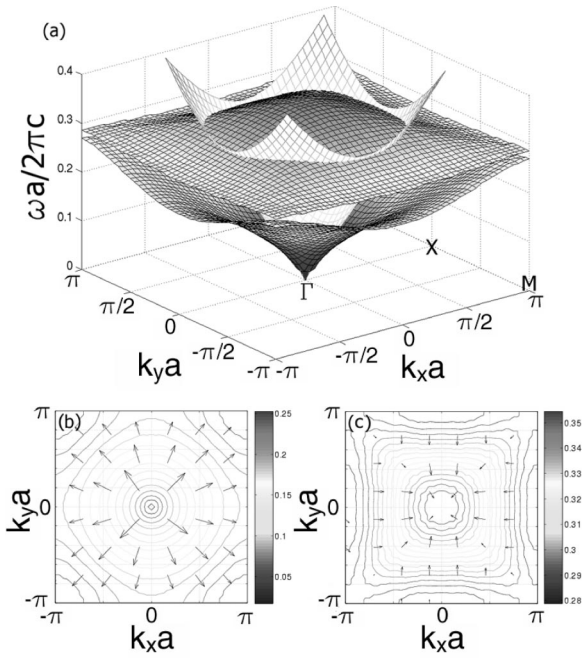

Fig. 2. (a) The dispersion, $\omega(k)$, relation (band-diagram) for the first two bands of the square PPC, calculated for all k-vectors in the first Brillouin zone. The light cone is represented as unshaded mesh. (b) The equifrequency contours for the first and (c) second bands. The vectors represent the gradient of frequency as the function of k_x and k_y (group velocity).

BZ. The band diagram was calculated from 325 equally spaced points in 1/8 of the I BZ [shaded region in the inset of the Fig. 1(b)], the data was then fitted using polynomial of the fifth order, and finally mapped into the entire I BZ. The light cone is represented by the unshaded mesh. From Fig. 2(a), we conclude that the first band is below the light cone (guided) in the whole frequency range, while the second band is guided only for normalized frequencies $a/\lambda < 0.306$. Furthermore, the 2nd band is almost flat and therefore light in that frequency range will be slowed down significantly. In Fig. 2(b) and (c), we plot the equifrequency contours of the first and second bands. $\vec{\nabla}_{\vec{k}}\omega$ is indicated by vectors along the equifrequency contours. Those vectors are oriented toward the Γ point in the case of the second band—an indication that the band is folded back into the first Brillouin zone. In addition, equifrequency contours of the second band are almost perfect squares in the frequency range where the second band is guided. This is very different from the unpatterned Si slab, where equifrequency contours of the guided modes are circles [Fig. 3]. This modification of the equifrequency contours from circles to squares leads to collimation-like effects in privileged directions (ΓX). We describe below this collimation effect that is intrinsic to this photonic crystal and is called self-collimation.

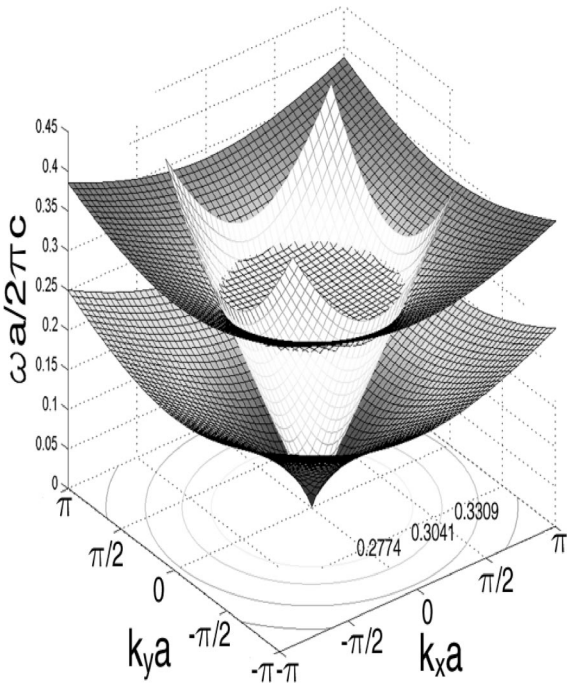

Fig. 3. The dispersion of the first two bands supported in the unpatterned Si slab. The light cone is represented as unshaded mesh. The equifrequency contours in the case of unpatterned slab are circles (shown for $a/\lambda = 0.2774$, 0.3041, 0.3309.) since all in-plane directions are equivalent.

In Fig. 4(a), we again show equifrequency contours of the second band of the square lattice PPC but this time only for frequencies that lie outside the light cone—$a/\lambda \in (0.273, 0.306)$. The light cone, for $a/\lambda = 0.306$, is represented by a dashed circle. It can be seen that the equifrequency contours can be approximated by squares for $a/\lambda \in (0.295, 0.306)$. The energy of the excited mode will propagate with a group velocity that can be calculated as

$$\vec{v}_g = \vec{\nabla}_{\vec{k}}\omega(\vec{k}) = \hat{x} \cdot \frac{\partial}{\partial k_x}\omega(k_x, k_y) + \hat{y} \cdot \frac{\partial}{\partial k_y}\omega(k_x, k_y). \quad (1)$$

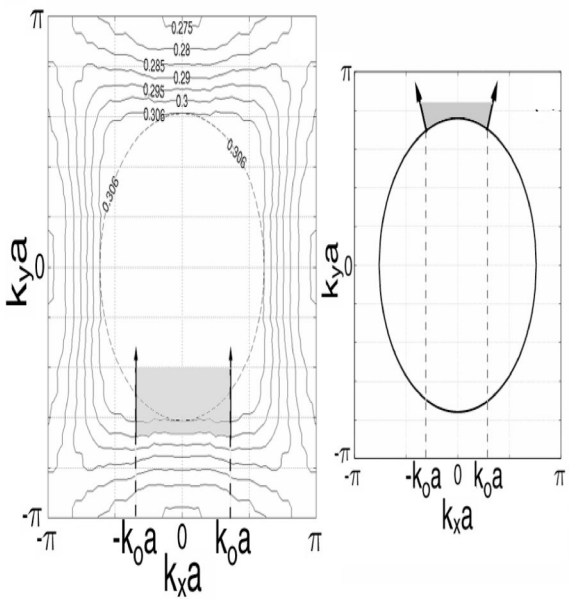

Fig. 4. (a) The equifrequency contours of the second band of a square lattice PPC. Only the region outside of the light cone is shown [$a/\lambda \in (0.273, 0.306)$]. The light cone, for $a/\lambda = 0.306$, is represented by the dashed circle. The light of frequency $a/\lambda = 0.3$ is self-collimated and propagates in the direction (in the real space) indicated by the gray color. (b) Equifrequency contours of the unpatterned Si slab are circles. Light diverges at the angles shown in the gray color.

It is useful to reformulate this equation in terms of normalized frequency a/λ and normalized k-vector $(a \cdot \vec{k})$, as band diagrams are usually shown in those dimensionless units. $\vec{v}_g = 2\pi c \vec{\nabla}_{\vec{k} \cdot a}(a/\lambda)$. The direction of propagation (in the real space) will be perpendicular to the equifrequency contour (in k-space). Therefore, if we consider light incoming from an unpatterned slab onto a PPC with a range of k-vectors so that k_x is between $-k_0$ and k_0 [Fig. 4(a)], light in the PPC will propagate along the y-axis direction (ΓX), as indicated by the gray color in Fig. 4(a). In other words, the light beam in the PPC can be self-collimated. This property of square PPCs is entirely due to the fact that equifrequency contours for the second band look like squares. In contrast to the PPC case, equifrequency contours of an unpatterned Si slab are circles [Fig. 4(b)]. When such a slab is excited with a range of k_x components, light in the slab diverges, as schematically indicated by the gray region in Fig. 4(b).

We consider a PC with a cleaved edge along the xOz plane and a light beam incident on the edge with an angle θ [Fig. 1(a)]. In our previous analysis we assumed that, for a given frequency, k_x is within one of the horizontal sides of the equifrequency "squares" [Fig. 4(a)]. However, the k_x component in the PC is determined by the wavelength of the incident light as well as the angle of incidence θ [Fig. 1(a)]. Therefore, we have to find the range of θ for which our assumption is valid. For an unpatterned slab, the relation between θ and k_x would be given by Snell's law, i.e., simply the conservation of the transverse k-vector component (k_x). In the case of an interface with a PC, k_x is only conserved modulo the reciprocal lattice basis vectors (the transverse component of all generated harmonics are of the form $k_x + n \cdot K$ where k_x is the transverse k-vector component of the incoming beam, n is an integer, and $K = 2\pi/a$). Indeed, at the air–Si interface, k_x is conserved, but multiple reflections in between the air holes and between the air holes and the PC edge complicate the problem. However, since the PC is a periodic structure, it conserves k_x modulo the reciprocal lattice basis vectors. Thus, neither the air–Si interface at the PC edge nor the multiple reflections between air holes can introduce Fourier components other than those that belong to the Bloch mode indexed by the transverse k-vector component. In other words, k_x is conserved in the first Brillouin zone.

In our case, the boundary is in the xOz plane, and therefore k_x and k_z are conserved. k_x can be expressed as $k_x = (2\pi/\lambda) \cdot \sin(\theta)$. In order for k_x to belong to a horizontal side of an equifrequency square, it has to satisfy $\mid k_x \mid \leq k_0$, where $2 \cdot (k_0 \cdot a)$ is the normalized length of the side of the square minus the rounded corners and is a function of normalized frequency. Combining these two expressions, we obtain

$$\frac{(k_0 \cdot a)}{(\frac{a}{\lambda}) \cdot 2\pi} \geq \mid \sin(\theta) \mid . \tag{2}$$

We will show that if the equifrequency contours were perfect squares, inequality (2) would be verified for all equifrequency contours below the light cone. We call k_0 the projection of the corner of the square on the k_x axis. Then the range of k_x components corresponding to self-collimated Bloch modes propagating in the x direction spans $2k_o$. Because the equifrequency contour is assumed to be a perfect square, k_0 is equal to the distance k_1 between the origin of the plot and the center of the side of the square $(k_1 = k_0)$. Because the equifrequency contour is below the light cone, $k_1/ge2\pi/\lambda$

$$\frac{(k_0 \cdot a)}{(\frac{a}{\lambda}) \cdot 2\pi} \geq 1. \tag{3}$$

Inequality (2) is then satisfied for any angle θ. That is, for any incident angle, light in the frequency range $a/\lambda \in (0.295, 0.306)$ can be self-collimated within the PPC and propagate along the y-axis direction (in real space).

However, this would only be true if the equifrequency contours were perfect squares. Since the equifrequency squares are rounded at the corners, we have to assume a more conservative value $k_{0,\min} \cdot a = 1.502$ for $a/\lambda = 0.306$ [Fig. 4(a)]. Then, the left-hand side of (2) becomes

$$\frac{(k_0 \cdot a)_{\min}}{(\frac{a}{\lambda}) \cdot 2\pi} = 0.817 \tag{4}$$

and $\mid \theta \mid \leq \arcsin(0.817) \approx 54^\circ$. Therefore, the square lattice PPC acts as a self-collimator for incident angles $\mid \theta \mid \leq 54^\circ$ and $a/\lambda \in (0.295, 0.306)$. The amount of light that is coupled into the slab depends on the incident angle. Also, the group velocity of a PC Bloch mode depends both on the normalized frequency and on the k-vector and is calculated to be in the range $v_g \in (0.16, 0.25) \cdot c_0$ (c_0 is the speed of light in vacuum) for $a/\lambda \in (0.295, 0.306)$ and $\mid \theta \mid \leq 54^\circ$.

In order to verify the predictions that self-collimation is possible in a square lattice PPC, we have used a 3-D FDTD modeling on such a structure. Fig. 5 shows the field evolution (B_z component) in an unpatterned (a) and patterned [(b) and (c)] Si slab. The structures were excited with a dipole source placed at

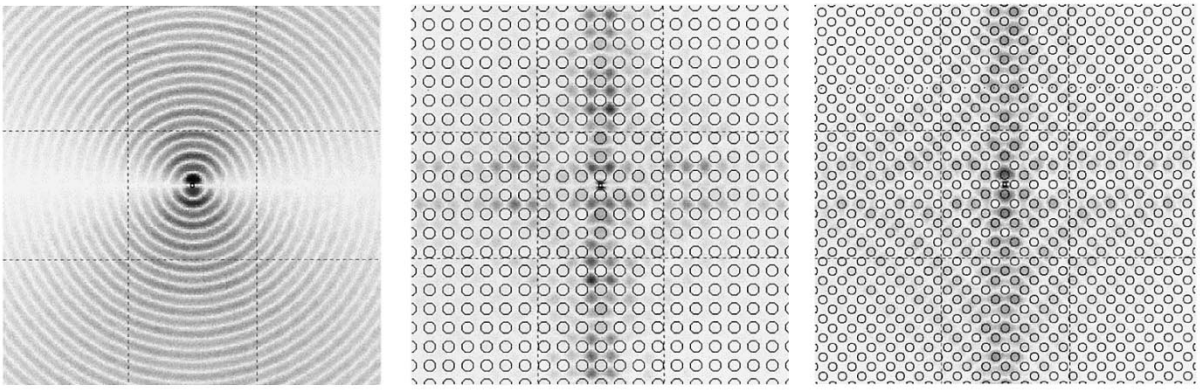

(a) (b) (c)

Fig. 5. Evolution of the B_z component of the EM-field excited in the (a) unpatterned slab and (b), (c) slab patterned with a square lattice PPC. The figure in (c) has been rotated and rescaled to show structural similarities between self-collimation in the first and second bands. Structures were excited with dipole sources (with E_x component) at frequencies (a) $a/\lambda = 0.295$, (b) $a/\lambda = 0.295$, and (c) $a/\lambda = 0.2086$. Self-collimation can be observed in case (b) as predicted. In this case, light is radiated predominantly along ΓX directions and correspond to modes of the second band. Radiation in y-*axis* direction is stronger because the structure was excited with E_x field only. In case (c), light is radiated mostly in the ΓM direction and corresponds to modes of the first band.

the center of the slab. In the case of the unpatterned slab, the characteristic dipole radiation, with spherical wavefronts, is observed [Fig. 5(a)]. The PPC structure shown in Fig. 5(b) was excited with a dipole source with a frequency ($a/\lambda = 0.295$) chosen to be in the frequency region of the second band where equifrequency contours are squares [Fig. 4(a)]. Because of that, it is expected that light is radiated predominantly in the four ΓX directions, that are perpendicular to the four sides of the equi-frequency "squares." Indeed, the 3-D FDTD simulation of the structure [Fig. 5(b)] shows such a behavior. We conclude that the square lattice PPC has modified the radiation pattern of the dipole source in the way predicted by the above analysis of equifrequency contours. It is also important to notice that this interesting phenomena is taking place outside the light cone. Therefore, the light is self-collimated as it propagates in the ideal PPC *without* any losses. Self-collimation can also be obtained by exciting the first band, this time light propagates in the ΓM direction, as shown in Fig. 5(c). This figure has been rotated by 45° and rescaled by $1/\sqrt{2}$ in order to show structural similarities between self-collimation in the first and second bands.

In summary, based on a 3-D FDTD analysis, we have found a range of parameters, PC geometry as well as frequency and incident angle of light, for which self-collimation can be observed. The next section is dedicated to phenomena that are more computationally intensive to explore. To this purpose, we first show that it is possible to adequately simulate self-collimation in a PPC through 2-D FDTD simulations. We then proceed with a more detailed analysis of equifrequency contours and validate our conclusions with corresponding 2-D FDTD simulations.

III. Extensive Analysis of Self-Collimation Based on 2-D FDTD

We have further extended our analysis based on the full dispersion diagram of a 2-D square lattice PC, here again obtained through the FDTD simulation of a unit cell. Because of the significantly less time-intensive calculations, we could achieve a much finer frequency resolution. We use the band diagram obtained through 2-D FDTD to set up 2-D simulations of self-collimated beams over much larger areas than was possible with the 3-D simulations and show phenomena that can only be seen after a long propagation distance. We increase the number of time steps per simulation to 2^{17} and map 630 equally spaced points in the irreducible Brillouin zone. The discretization is 45 points per lattice period, amounting to 2025 points per unit cell.

A. Applicability of a 2-D FDTD Analysis to PPCs

In order to accurately predict the frequencies of the bands of a PPC 3-D structure using 2-D calculations, it is desirable to use the effective index method in a 2-D simulation [Fig. 6(a)]. However, we find that there is a tradeoff between minimum distortion of the shape of the bands ($n_{\text{eff}} = 3.5$) and best overall frequency overlap ($n_{\text{eff}} = 2.7$). It can be seen that while the bands resulting of an effective index of 2.7 are roughly in the same frequency range as the bands of the 3-D PPC of index 3.5, their shape is highly distorted. Therefore, we propose an alternative method in which the same index is used as in the 3-D case ($n = 3.5$), resulting in minimally distorted bands, and then constant frequency offset is added [Fig. 6(b)]. A constant normalized frequency offset of 0.0533 results in the best overlap between 2-D and 3-D calculations. For normalized frequencies between 0.15 and 0.35, there is a very close overlap. We conclude that we can adequately predict the self-collimation or the superprism behavior of the PPC through 2-D simulations by adding a constant frequency offset. In the following two sections, 2-D FDTD simulations were used for this purpose. In order to relate it to a 3-D PPC, the frequency offset must be added to all reported frequencies.

B. Group Velocity and Group Velocity Dispersion

The maximum group velocity in the second band is calculated to be 0.276 times the speed of light and is reached in the region of strong self-collimation, where the equifrequency contours are squares with maximally flat sides [Fig. 7]. This region also corresponds to a local minimum of the group velocity dispersion (GVD), as the group velocity goes through its maximum value. Thus, a self-collimated beam in that regime (minimum spatial pulse dispersion) would also have maximum group velocity and

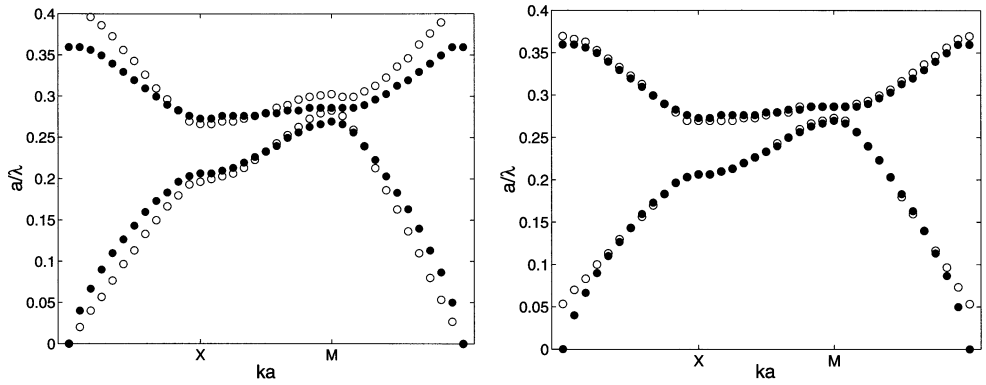

Fig. 6. (a) The band-diagram for TE-like (vertically even) modes of the square lattice PPC with index 3.5 (dots) and the TE modes for the 2-D square lattice PC (circles) with an effective index of 2.7. (b) The band diagram for TE-like modes of the square lattice PPC with index 3.5 (dots) and the TE modes for the 2-D square lattice PC (circles) with an index of 3.5 and an added frequency offset of 0.0533.

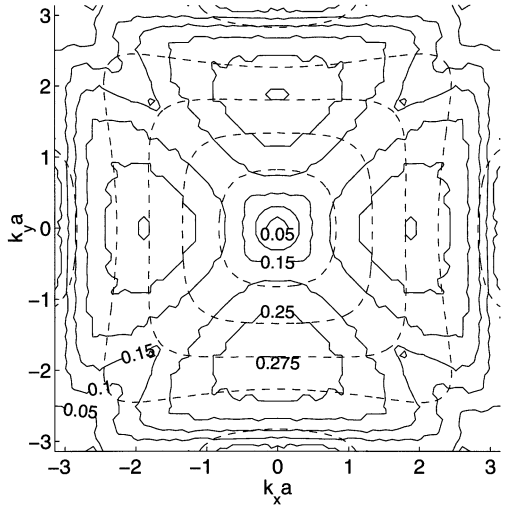

Fig. 7. The equifrequency contours of the second TE-like band (dashed lines) and the isocurves for group velocity (continuous line). The group velocity is given in a fraction of the vacuum speed of light. The contours of constant group velocity are ragged because they correspond to the numerical differentiation of the raw data.

minimum GVD (temporal pulse dispersion). This is for a normalized frequency $a/\lambda = 0.261$ and a normalized k-vector $k \cdot a = 1.795$ in the ΓX direction. It correspond to an effective index of 1.096, thus, if this PC mode had the same k-ω in the 3-D PPC, it would be below the light cone. However, in the case of a 3-D planar photonic crystal, the frequency is shifted up (in the case of the PPC analyzed in the previous section by 0.0533). This mode is then situated inside the light cone and is leaky. That is why in the 3-D analysis the maximum v_g for nonleaky modes was found to be 0.25 instead of 0.276 predicted by 2-D calculation. In other words, in a PPC as described in the above section, we need to use a nonoptimum mode in terms of GVD, maximizing v_g and strongest self-collimation in order to stay below the light cone or we would have to accept a finite amount of losses because of leaky modes. In order to make a rational design decision, those losses need to be further evaluated. As those modes remain close to the boundary of the light cone, and most of the power of those modes is contained in higher order harmonics that are outside the light cone, losses could be relatively low.

In the fiber optics literature, the GVD is given by β_2 as

$$\beta_2 = \frac{\partial}{\partial\omega}\left(\frac{1}{v_g}\right) = -\frac{1}{v_g^2}\frac{\partial v_g}{\partial\omega}. \tag{5}$$

The pulse broadening (time) is given by

$$\frac{\partial v_g}{\partial\omega}\Delta\omega\frac{L}{v_g^2} \tag{6}$$

where L is the propagation distance and $\Delta\omega$ is the pulsewidth in ω. We multiplied Δ_{v_g} by the propagation time L/v_g in order to get the pulse broadening in units of distance, then we divided by v_g to get the pulse broadening in units of time. In terms of β_2 the pulsewidth (time) is given by

$$\mid \beta_2 \mid \cdot L \cdot \Delta\omega \tag{7}$$

where β_2 is correctly defined because $v_g = v_g(\omega)$ in a fiber. However, in a PC and in the case of self-collimation, v_g depends both on ω and on the specific k-vector on the equifrequency contour. We can define a similar parameter in the case of a PC by defining $v_g(\omega)$ as the group velocity for the center point of the side of the squarish equifrequency contour, i.e., for the central *k-vector* of the beam. Then

$$\frac{\partial}{\partial\omega}(v_g) = \frac{\vec{\nabla}_k(v_g)\cdot\vec{\nabla}_k(\omega)}{v_g^2}. \tag{8}$$

We take the gradient of the group velocity by k, project the gradient on the energy propagation direction by taking the scalar product with $\vec{v_g}/v_g$, and divide by v_g to convert the derivative by k in a derivative by ω. Again, this derivative is only defined because we take a particular $v_g(\omega)$. We then define β_2 as

$$\beta_2 = \frac{\partial}{\partial\omega}\left(\frac{1}{v_g}\right) = -\frac{\vec{\nabla}_k(v_g)\cdot\vec{\nabla}_k(\omega)}{v_g^4} \tag{9}$$

$$\mid \beta_2 \mid \leq \frac{\parallel \vec{\nabla}_k(\omega) \parallel}{v_g^3}. \tag{10}$$

β_2 then gives the broadening for a pulse consisting of Bloch modes with a range of k_y's, but with $k_x = 0$. There is a second

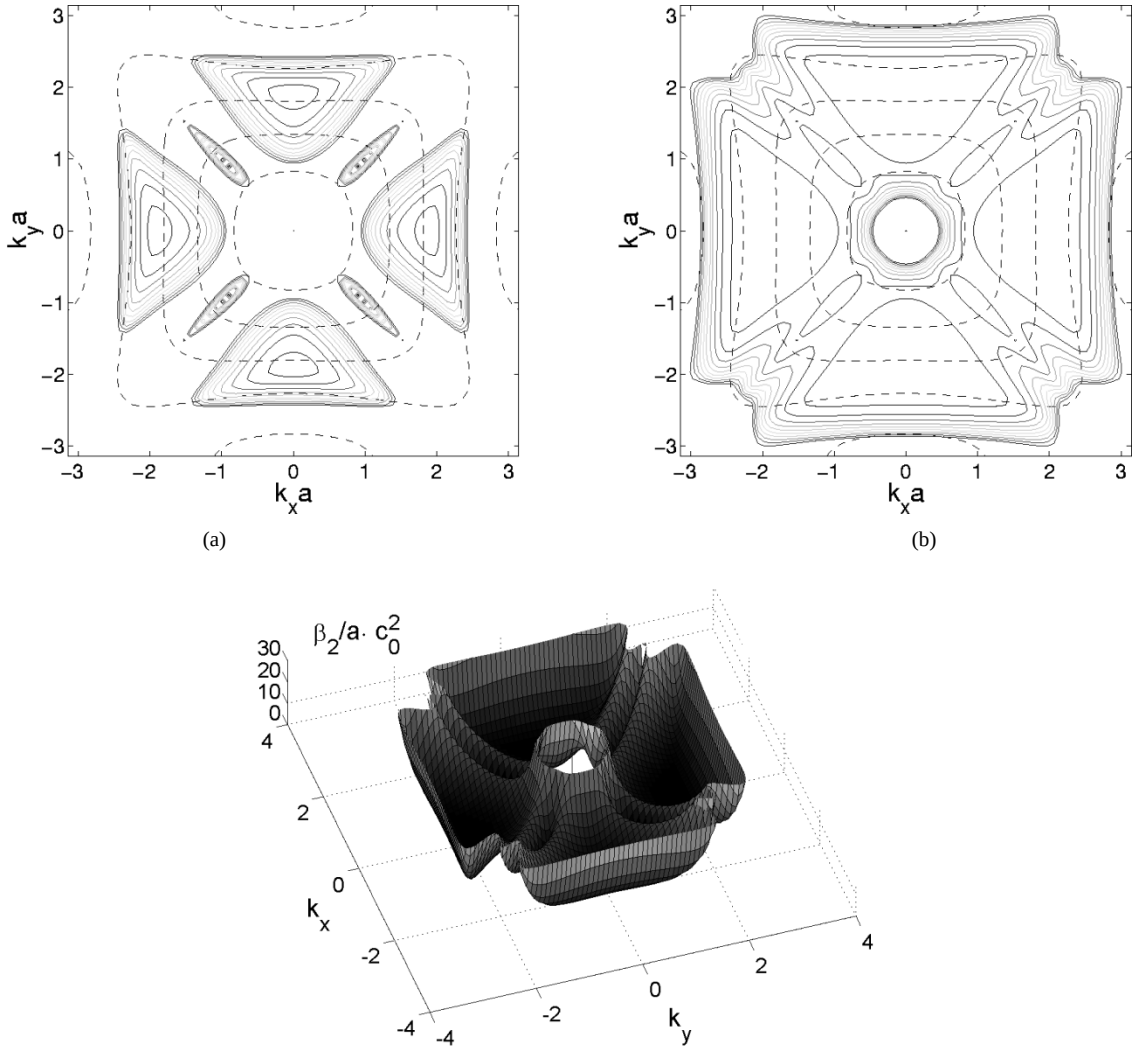

Fig. 8. Isocurves for $\beta_2/a \cdot c_0^2$ (dimensionless normalized units) for the second band of a square lattice PC with $r/a = 0.3$. The group velocity calculated previously was smoothed before further differentiation. (a) Isocurves for $\beta_2/a \cdot c_0^2$ from 0 to 10 (dimensionless normalized units) and (b) isocurves for $\beta_2/a \cdot c_0^2$ from 10 to 100. (c) A 3-D plot of the same data, for better visualization.

temporal pulsewidth broadening mechanism that must be taken into account. It is due to the change of group velocity of components of the same frequency, but with different k-vectors. This time we must take into account the component of $\vec{\nabla}_k(v_g)$ that is transverse to the direction of propagation, $(\vec{\nabla}_k(v_g))_t$. Then the pulse broadening is given by

$$(\vec{\nabla}_k(v_g))_t \cdot (\Delta_k)_t \cdot \frac{L}{v_g^2} \leq \frac{\| \vec{\nabla}_k(v_g) \|}{v_g^3} \cdot (v_g \cdot (\Delta_k)_t \cdot L) \quad (11)$$

where $(\Delta_k)_t$ is the transverse k range of the pulse. The total pulse broadening is then smaller than

$$\frac{\| \vec{\nabla}_k(v_g) \|}{v_g^3} \cdot (L \cdot \Delta_\omega + L \cdot (\Delta_k)_t \cdot v_g) \quad (12)$$

$$\frac{\| \vec{\nabla}_k(v_g) \|}{v_g^3} \cdot L \cdot ((\Delta_k)_t + (\Delta_k)_l) \cdot v_g. \quad (13)$$

This formula is suboptimum in that it assumes the maximum gradient for the GVD in both the k_x and k_y directions, but it has the merit to give a scalar to characterize GVD (instead of a 2 by 2 matrix). We than redefine β_2 as

$$\beta_2 = \frac{\| \vec{\nabla}_k(v_g) \|}{v_g^3}. \quad (14)$$

As shown above, the group velocity is a function of normalized frequency and normalized k-vector, but $\vec{\nabla}_k$ is not. Thus, β_2 is dependent on the scaling of the PC, but β_2/a is independent of the lattice parameter a (Fig. 8).

C. Beating Patterns

Because the equifrequency contours are squares with rounded corners and slightly concave sides, the group velocity has a small angular divergence from the normal to the side of the square, which leads to limited diffraction. There are only three points along each side with a group velocity exactly perpendicular to the side of the square [Fig. 9]. If we excite a self-collimated beam with a wide enough range of k-vectors to cover

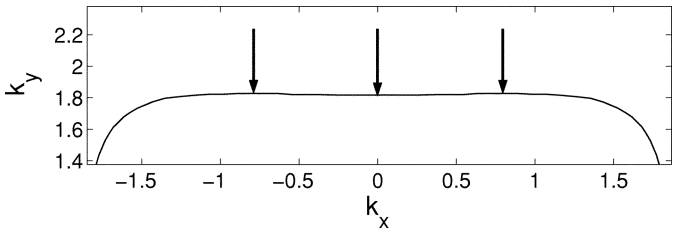

Fig. 9. Zoom on one of the sides of the equifrequency contour's "square" at normalized frequency 0.2596. The arrows indicate the k-vectors for which the group velocity is perfectly aligned to the y axis.

all of those three Bloch modes and all the Bloch modes in between, we expect the self-collimated beam to be dominated by those three components after a finite propagation distance. This can, for example, be achieved with a dipole source, a narrow waveguide, or a light spot from a lens with high numerical aperture. On the other hand, a collimated Gaussian beam from free space will have a narrow range of k-vectors, so that at most one of the three perfectly collimated Bloch modes will be excited. This is important, because in the first case interference between the three main components will create an interference pattern, while in the latter there will be no such pattern. We verified this by taking the spatial Fourier transform of the field in a region of $15 \cdot 15$ periods, centered around the self-collimated beam ($a/\lambda = 0.2596$) after propagating for 400 periods. The self-collimated beam was excited by a dipole source centered on one of the holes. The three perfectly collimated components are strongly dominant [Fig. 10].

The central component has a slightly smaller value of k_y than the two other components. Thus, we expect to see a beating pattern due to δk_y along the direction of propagation (y). To test this, we propagated a self-collimated beam of normalized frequency 0.2596 (distributed 2-D FDTD). We could observe a beating pattern with a beating length of about 1000 lattice periods (this corresponds to $\delta k_y = 2 \cdot \pi/1000 = 0.0063$, for a δk_y of 0.0093 taken from the equifrequency contour). In order to confirm that the beating length can be related to δk_y, we propagated a self-collimated beam of $a/\lambda = 0.25$ and found a beating length of 133 periods (this corresponds to $\delta k_y = 2 \cdot \pi/133 = 0.047$ for a δk_y of 0.057 taken from the equifrequency contour).

We also observed in both cases the appearance of side lobes. (The beating lengths reported above are unambiguously defined by the intensity profile at the center of the self-collimated beam.) This is a transverse interference pattern due to the different k_x of the three perfectly collimated components. The transverse interference pattern can only be seen if the self-collimated beam is wide enough after significant broadening. As the continuum of Bloch-modes that give the continuum of k_x components responsible for the finite beam width converges to the superposition of three discrete modes, the beam broadens ($\Delta k_x \cdot \Delta x \geq 2\pi$) and an interference pattern emerges. In the case of $a/\lambda = 0.2596$, this interference pattern has a width of $2 \cdot \pi/1.16 = 5.4$ and in the case of $a/\lambda = 0.25$ a width of $2 \cdot \pi/1.38 = 4.5$. A tiling pattern is generated by the simultaneous effect of both interferences, beating along the direction of propagation and transverse interference pattern. Because $\delta k_y \ll \delta k_x$, the beating length in the y direction is much larger than the period of the transverse interference pattern and the overall effect is one of a comb of

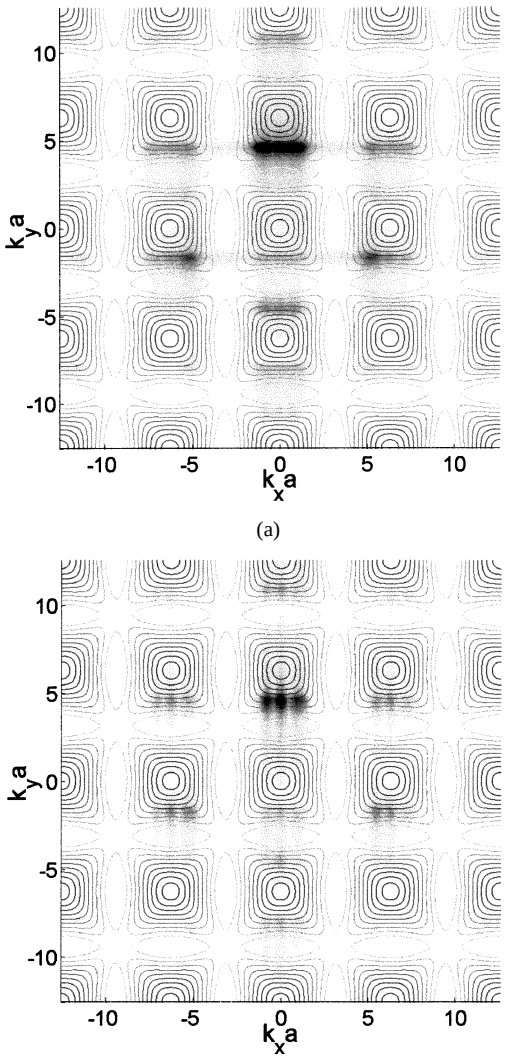

Fig. 10. (a) The spatial Fourier transform of a self-collimated beam at normalized frequency 0.2596 after 30 periods and (b) after 400 periods. Three discrete components become dominant. The equifrequency contours are overlaid.

side lobes that offsets by half the period of the transverse interference pattern every half longitudinal beating length. Fig. 11 shows the emerging lateral interference pattern as well as the longitudinal beating. In order to correctly resolve the side lobes, very wide PCs must be simulated. Because of computational limitations we changed the discretization to 22 points per unit cell for this calculation. This computational change introduced a 1% frequency down shift of the bands (0.003 in units of normalized frequency) around $a/\lambda = 0.2596$. Because the beating length changes as $1/\delta k_y$, and δk_y approaches zero, the beating length is very sensitive to frequency in this region.

It is important to take this beating into account if self-collimation is to be used in real devices. For example, if the self-collimated beam is to be coupled out to a waveguide, it is important to know that the field might have a minimum at the center of the self-collimated beam. Moreover, a self-collimated beam is not like a waveguide mode that propagates unchanged down a waveguide. The analogy would hold only for a self-collimated beam corresponding to a perfectly flat equifrequency contour.

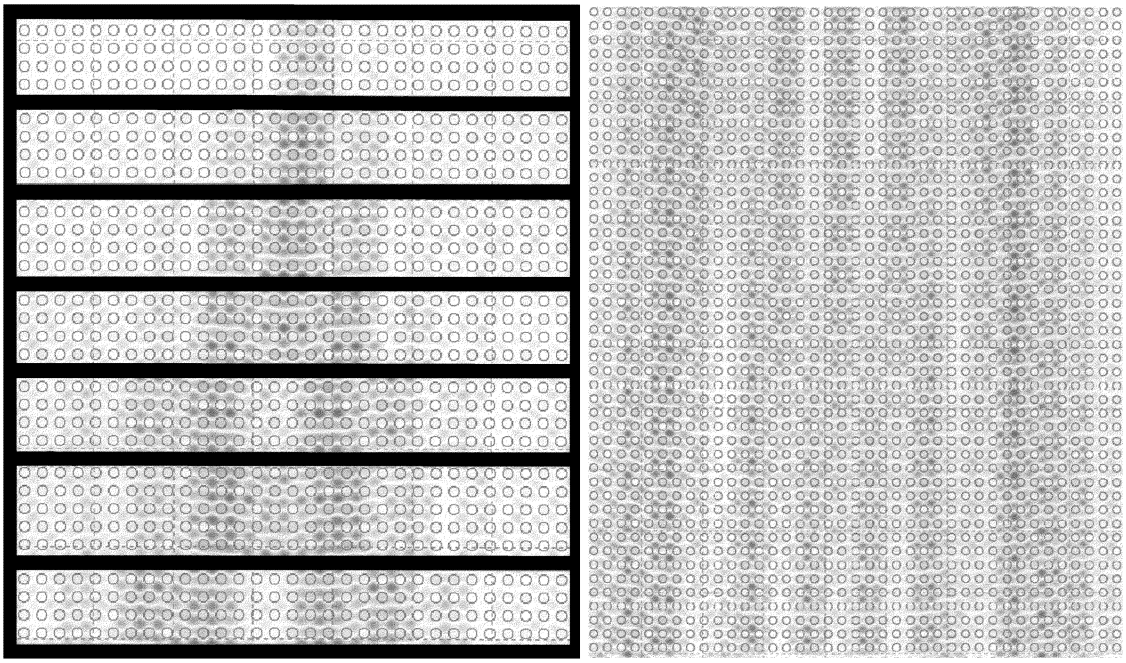

(a) (b)

Fig. 11. (a) Self-collimated beam ($a/\lambda = 0.2596$) after different propagation distances (top down: 30, 80, 130, 180, 230, 280 and 330 lattice periods). The self-collimated beam broadens and a beating pattern appears. (b) Self-collimated beam ($a/\lambda = 0.25$) after 220 lattice periods propagating down. The beating pattern and the transverse interference pattern are clearly seen: the comb of lobes correspond to the transverse beating pattern, the offset of the comb between the top and the bottom of the picture is due to the longitudinal beating. If a vertical line is drawn in the center of the figure, the intensity profile corresponds to beating in the common terminology. Light on the sides of the beam corresponds to weakly self-collimated light that disperses out of the beam. Because of the broadening of the beam, there are more lobes on the lower end of the picture. For both (a) and (b) we took 22 computation points per unit cell.

However, because the equi-frequency contours are only approximately flat, a diffraction-limited length limits self-collimation for a practical device.

So far we have analyzed self-collimation in the second band of a square lattice PPC. However, light can also be self-collimated in the first band of a square lattice PC, but in the ΓM direction this time. In the next subsection, we will show that a self-collimated beam can even be transmitted from the first band to the second band with low losses and low distortion. We will investigate structural similarities (in reciprocal space) between self-collimation in the first and second bands.

D. Comparative Analysis of Self-Collimation in the First and Second Bands

The first and second bands of a square lattice PPC seem to have very different structures. Indeed, the group velocity points out of the equifrequency contours in the first band, while in the second band it points inside. Also, self-collimation takes place in the ΓM direction in the first band and in the ΓX direction in the second band. However, we can show that the two bands are related by a simple transformation, consisting of a 45° rotation and a rescaling. In particular, the regions where self-collimation takes place, where the sides of the equifrequency contours are flat, have the same structure in both bands. Indeed, the reciprocal space transformation maps those two regions one onto another, except for a slight frequency offset (0.007 in units of normalized frequency).

In order to show this we will introduce a second PC (PC2), that is in fact the same PC rescaled and rotated, and show similarities between the two PCs. The transformation in real space that maps PC1 on PC2 is the real space equivalent of the inverse space transformation mentioned previously. By showing that the second band of PC1 overlaps with the first band of PC2, we show that the second band of a square lattice PPC has the same structure as the corresponding zone of the first band.

We define the second PC 2 (PC2) as a square lattice 2-D PC with lattice constant $a/\sqrt{2}$ (where a is the lattice period of photonic crystal 1), hole radius $r/\sqrt{2}$ (where r is the hole radius of PC1), and with a lattice rotated by 45° in respect to photonic crystal 1 (PC1). r/a is conserved, the bands of PC2 are obtained by rotating the bands of PC1 by 45° and the bands are rescaled according to (15) and (16). The real space dimensions have also been rescaled by $1/\sqrt{2}$, ant therefore the k-vectors are rescaled by $\sqrt{2}$. The area of the first Brillouin zone of PC2 is then twice the area of the 1st Brillouin zone of PC1 [Fig. 12(b)]. It contains both the first Brillouin zone and the second Brillouin zone of PC1 (the second Brillouin zone of PC1 is composed by the four"corners" of the Brillouin zone of PC2)

$$\vec{k_2} = \sqrt{2} \cdot rot_{45^\circ}(\vec{k_1}) \tag{15}$$

$$\left(\frac{a}{\lambda}\right)_2 = \left(\frac{a}{\lambda}\right)_1 \sqrt{2}. \tag{16}$$

From here on, the first and second Brillouin zones will refer to the first and second Brillouin zones of PC1. We can see from Fig. 12(a) and (b) that the second band of PC1 overlays onto the first band of PC2 in the second Brillouin zone. We can also see from Fig. 12(c) that the first band of PC1 overlays with the first band of PC2 in the first Brillouin zone. This is further illustrated by Fig. 12(c), that shows the first and second bands

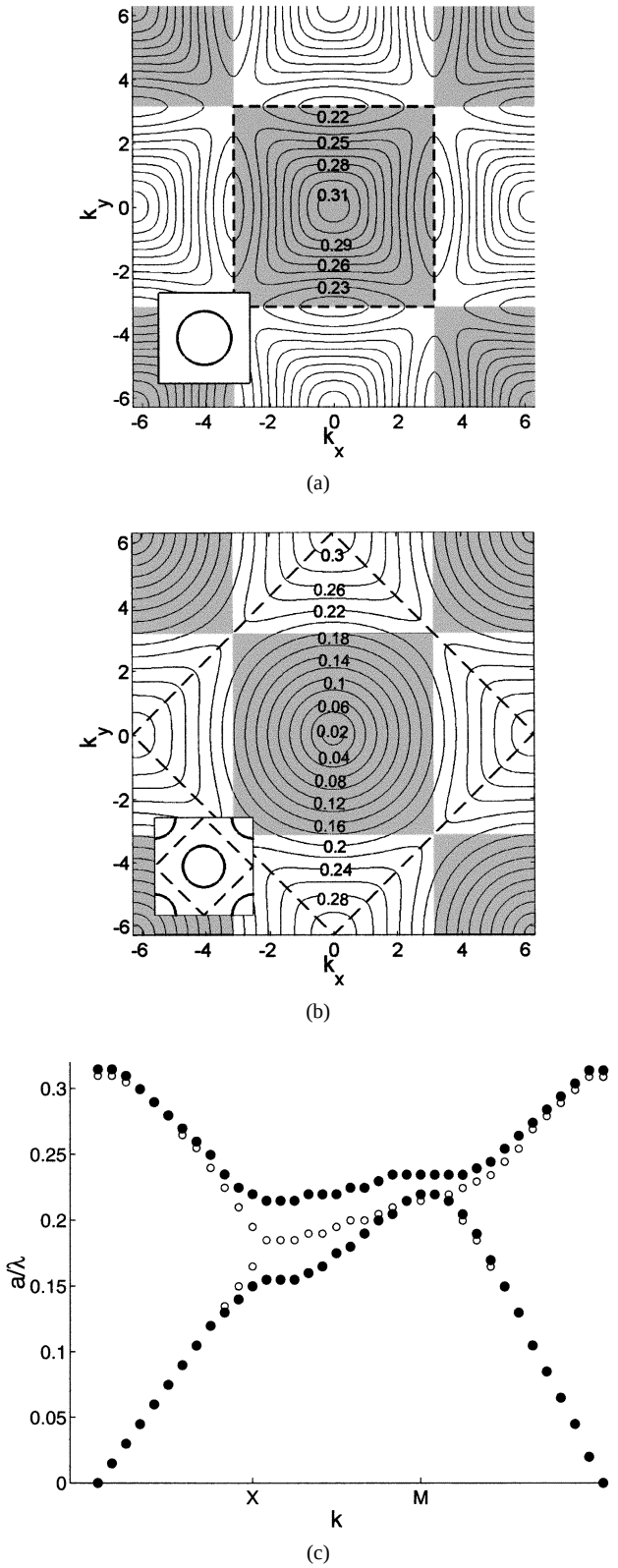

Fig. 12. Equifrequency contours of (a) the second band of PC1 and of (b) the first band of PC2 and unit cells (insets). The dashed line in (b) shows the first Brillouin zone of PC2. The shaded region corresponds to where the band structures differ, and the white region to where they are the same. (c) The first and second bands of PC1 (dots) and the first band of PC2 (circles). The first band of PC2 is folded back into the first Brillouin zone of PC1. The labels X and M refer to the high symmetry points of PC1 (the labels would need to be interchanged for PC2, that has been rotated). The band structures of the two photonic crystals are very close other than in the frequency domain around the bandgap.

of PC1 (dots) and the first band of PC2 (squares) folded back in the first Brillouin zone of PC1. The only frequency region where the two band structures strongly differ is along XM direction of PC1.

As already mentioned, the structural similarities between PC1 and PC2 arise from structural similarities between the first and second bands of PC1. The transformation from PC1 to PC2 is the real space equivalent to the transformation from the first to the second band. One of the consequences of this structural similarity is that a beam self-collimated in the first band with normalized frequency a/λ will show exactly the same beating pattern as a beam self-collimated in the second band with normalized frequency $\sqrt{2}\cdot a/\lambda$, modulo a 45° rotation and a rescaling.

There is a slight frequency offset as PC1 and PC2 overlay closely, but not perfectly. The equifrequency contour corresponding to the second band of PC2 at $a/\lambda = 0.2596$ overlays the equifrequency contour of the first band of PC1 at $a/\lambda = 0.2526$ (2.7% offset). We can compensate this frequency offset for $a/\lambda = 0.2596$ by using a hole radius of $r/\sqrt{2} = 0.322\cdot a/\sqrt{2}$ for PC2 instead of $0.3\cdot a/\sqrt{2}$. In the following discussion this hole radius compensation is applied.

We compare the width of a beam of normalized frequency $a/\lambda = 0.2596$, self-collimated in the second band of PC1 ($r/a = 0.3$), with the width of a beam of normalized frequency $a/\lambda = 0.2596/\sqrt{2} = 0.1836$, self-collimated in the first band of a PC of same lattice period a and with $r/a = 0.322$. The beams are excited by a dipole source predominantly radiating in ΓX ($a/\lambda = 0.2596$) and the ΓM ($a/\lambda = 0.1836$) directions and located in the center of one of the holes. The respective rms of the beams [(17)] are $2.3060\cdot a$ and $2.7881\cdot\sqrt{2}\cdot a$, respectively

$$\frac{\sqrt{\int X^2\cdot B_z^2}}{\sqrt{\int B_z^2}} \tag{17}$$

$$\frac{\text{rms}_{1^{st}\text{band}}}{\text{rms}_{2^{nd}\text{band}}} = \sqrt{2}\cdot 1.21. \tag{18}$$

The ratio between the beam widths [(18)] could lead to the erroneous conclusion that self-collimation is significantly stronger in the second band. However, if a beam of normalized frequency $a/\lambda = 0.1836$ were to be self-collimated in the second band instead of the first, the PC would need to be rescaled to a lattice constant of $a\sqrt{2}$, rescaling the rms by $\sqrt{2}$ at the same time. Collimating a beam in the first band is thus similar to collimating a beam in the second band. However it is easier to fabricate a PC so that a given frequency is self-collimated in the second band, as the lattice constant is $\sqrt{2}$ times larger, requiring less demanding lithography. These conclusions can also be applied to a 3-D photonic crystal: in Fig. 5, we showed a self-collimated beam in the 2nd band at $a/\lambda = 0.295$ and in the first band at $a/\lambda = 0.295/\sqrt{2} = 0.2086$.

The second practical consequence is that a self-collimated beam can be transmitted almost undistorted between photonic crystals of type 1 and type 2, and PC1 and PC2 have a lattice matched interface, as shown in Fig. 14. As they have the same band structure in the second Brillouin zone of PC1, we could be tempted to conclude that they have similar Bloch modes, and thus a good interface. However, this is not necessarily true, since

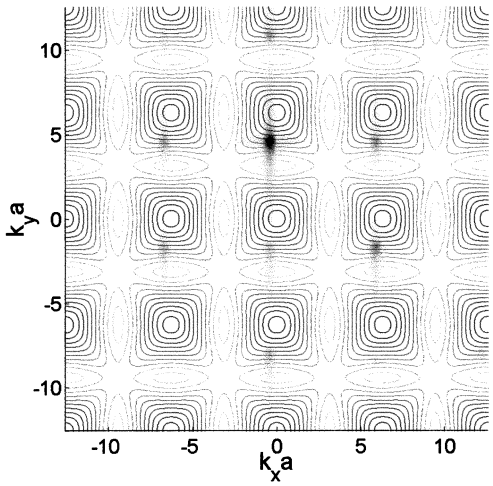

(a)

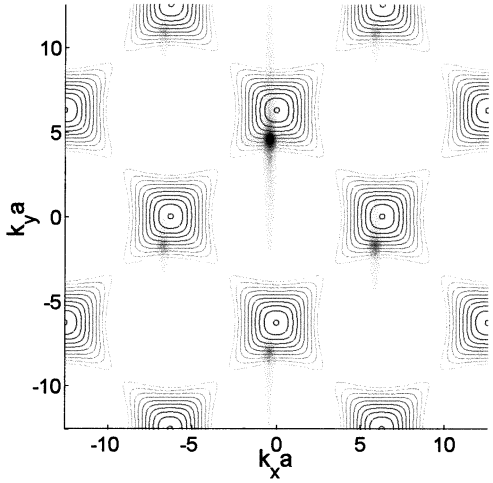

(b)

Fig. 13. (a) Spatial Fourier transform for a Bloch mode of PC1 and (b) for the mode of PC2 that has approximately the same normalized frequency and k-vector in the second Brillouin zone of PC1. Equifrequency contours in the normalized frequency range 0.22 to 0.31 (second band of PC1) are overlaid. It can be seen that the Bloch mode of PC1 differs from the Bloch mode of PC2 in that it has components in the first Brillouin zone of PC1, however those components only make up a small fraction of the power in the Bloch mode.

Bloch modes have more than one spatial Fourier component (see Fig. 13). They are indexed by the Fourier component inside the first Brillouin zone, but have Fourier components shifted from the "base" component by an integer number of reciprocal lattice basis vectors ($n \cdot K_1 + m \cdot K_2$, where n and m are integers, $K_{i,j} \cdot e_{i,j} = \delta_{i,j}$, $e_{i,j}$ are the real space lattice vectors and $\{i,j\} = \{1,2\}$). This results from the general form of a Bloch mode given as

$$A_{i,k}(x,y) \cdot e^{i(k_x x + k_y y)} \tag{19}$$

where $A_{i,k}(x,y)$ has the same periodicity as the PC (period a in x and in y) and i indexes the photonic band. Because of this periodicity, the Fourier transform of $A_{i,k}(x,y)$ has only components in k and in $k + n \cdot K_1 + m \cdot K_2$

$$A_{i,k}(x,y) \cdot e^{i(k_x x + k_y y)} = \sum_{n,m} A_{i,k;n,m} \cdot e^{i(k + n \cdot K_1 + m \cdot K_2) \cdot (x \cdot e_x + y \cdot e_y)} \tag{20}$$

$$A_{i,k}(x,y) \cdot e^{i(k_x x + k_y y)} = \sum_{n,m} A_{i,k;n,m} \cdot e^{i(k + n \cdot 2\pi/a)x + i(k + m \cdot 2\pi/a)y}. \tag{21}$$

Thus, having the same k-ω in one Brillouin zone is not sufficient for comparison. Modes of PC1 and PC2 with the same k-vector in the second Brillouin zone (of PC1) will differ in the first Brillouin zone. The PC1 mode will have a Fourier component in the first Brillouin zone of PC1 while the PC2 mode will not. Both the first and second Brillouin zone of PC1 are within the first Brillouin zone of PC2, thus a Bloch mode of PC1 has two harmonics in the first Brillouin zone of PC2, while PC2 has only one. However, the ratio between the power in the Fourier component in the first Brillouin zone and the power in the harmonic in the second Brillouin zone was calculated to be 0.057 for a typical self-collimated mode of PC1 (second band). This means that even though modes of PC1 have harmonics in the first Brillouin zone of PC1 and equivalent modes of PC2 have not, this difference only includes a very small fraction of the total power in the mode. A similar analysis has already been reported for PC waveguides [19], [20].

It is interesting to notice that the energy of the Bloch mode propagates in the opposite direction than the k-vector corresponding to the small Fourier component in the first Brillouin zone. Because the mode is referenced by this k-vector, the group velocity is negative in a formal way. However, it can be seen that this has no real physical meaning as most of the power of the Bloch mode is contained in harmonics with k-vectors that point in the same direction as the group velocity.

We did not conduct a quantitative analysis of what happens to the power contained in the weak harmonic in the first Brillouin zone of PC1. However it is interesting to note that it has the same k_x component (k-vector component transverse to the interface) as the dominant harmonics, and as such as the harmonics of the Bloch mode in PC2. If we consider PC1 and PC2 as metamaterials with a boundary problem, conservation of the transverse k-vector component (k_x) is not contradictory to the transmittance of the weak component. Of course this is only a qualitative analogy as PC1 and PC2 are mesoscopic structures.

Next, we simulated a beam propagating from crystal 1 to a crystal of type 2. At the junction between PC1 and PC2, we introduced an extra line defect $\delta/a = 0.14$ that optimized the rms of the self-collimated beam in PC2 after crossing the interface. We found that in the best case the rms after the interface was 1.07 times the rms before the interface (surprisingly this is a smaller beam width than for a beam directly excited by a dipole under the above conditions) and that 94% of the power was transmitted. For a PC with slightly larger holes and an open bandgap, this can provide a low-loss interface away from the bandgap combined with the possibility to use the bandgap in a reflector configuration. The interface between those two PCs could be generalized to triangular lattice PCs by using a 30° rotation and by rescaling the lattice period by $1/\sqrt{3}$.

IV. Conclusion

We have conducted a 3-D analysis of self-collimation and gave a range of parameters that make it possible to experimentally explore self-collimation in a planar photonic crystal. We

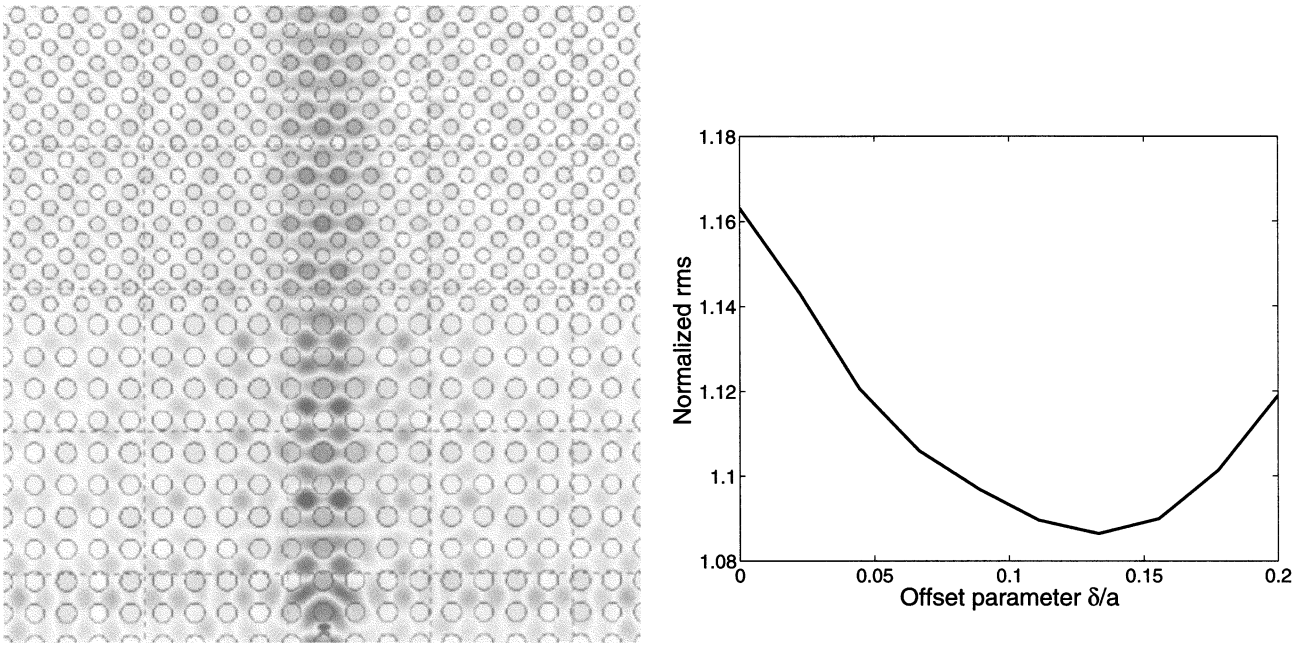

(a) (b)

Fig. 14. (a) Self-collimated beam at frequency $a/\lambda = 0.2596$ that propagates from PC1 ($r/a = 0.3$) to PC2 ($r = 0.322/\sqrt{2}a$). (b) rms of the self-collimated beam in PC2 after crossing the boundary, after crossing the boundary. The rms of the beam is normalized by the rms before the interface.

showed how a 2-D analysis could be used to reproduce results from 3-D PPCs by using a 2-D calculation with a frequency offset. For the PC investigated in this paper, optimum self-collimation was found to take place inside the light cone and, thus, in an intrinsically lossy region. In-depth analysis of self-collimation, based on analysis in the reciprocal space, was performed. We showed the occurrence of beating patterns and beam broadening that must be taken into account when designing devices based on self-collimation. Finally we showed that it is possible to make a low-loss interface between two square lattice PCs with different orientations, again achieved by matching the Bloch modes in reciprocal space. We suggested that this interface might be used in integrated optics in order to build multifunctional PBG structures. In a future publication, we will address a way to interface self-collimation-based devices with more conventional integrated optics.

ACKNOWLEDGMENT

The authors would like to acknowledge T. Baehr-Jones from Luxtera, Inc., for the development of the distributed 3-D FDTD code and to thank Luxtera, Inc., for making computing power available.

REFERENCES

[1] E. Yablonovitch, "Inhibited sponaneous emission in solid-state physics and electronics," *Phys. Rev. Lett.*, vol. 58, pp. 2059–2062, 1987.

[2] T. F. Krauss, R. M. De La Rue, and S. Brand, "Two-dimensional photonic-bandgap structures operating at near infrared wavelengths," *Nature*, vol. 383, pp. 692–702, 1996.

[3] S. G. Johnson, S. H. Fan, P. R. Villeneuve, J. D. Joannopoulos, and L. A. Kolodziejski, "Guided modes in photonic crystal slabs," *Phys. Rev. B*, vol. 60, pp. 5751–5758, 1999.

[4] D. Labilloy, H. Benisty, and C. Weisbuch *et al.*, "Quantitative measurement of transmission, reflection, and diffraction of two-dimensional photonic band gap structures at near-infrared wavelengths," *Phys. Rev. Lett.*, vol. 79, p. 4147, 1997.

[5] O. Painter, R. K. Lee, A. Yariv, A. Scherer, J. D. O'Brian, P. D. Dapkus, and I. Kim, "Two-dimensional photonic band-gap defect mode laser," *Science*, vol. 284, pp. 1819–1821, 1999.

[6] veguiding in planar photonic crystalsM. Lončar, D. Nedeljković, T. Doll, J. Vučković, A. Scherer, T. P. Pearsall, and T. P. Pearsall, *Appl. Phys. Lett.*, vol. 77, pp. 1937–1939, 2000.

[7] C. J. M. Smith, R. M. De La Rue, and M. Rattier *et al.*, "Coupled guide and cavity in a two-dimensional photonic crystal," *Appl. Phys. Lett.*, vol. 78, pp. 1487–1489, 2001.

[8] S. Noda, A. Chutinan, and M. Imada, "Trapping and emission of photons by a single defect in a photonic bandgap structure," *Nature*, vol. 407, pp. 608–610, 2000.

[9] B. Gralak, S. Enoch, and G. Tayeb, "Anomalous refractive properties of photonic crystals," *J. Opt. Soc. Amer. B*, vol. 17, pp. 1012–1020, 2000.

[10] E. Silvestre, J. M. Pottage, P. S. J. Russell, and P. J. Roberts, "Design of thin-film photonic crystal waveguides," *Appl. Phys. Lett.*, vol. 77, pp. 942–944, 2000.

[11] H. Kosaka, T. Kawashima, A. Tomita, M. Notomi, T. Tamamura, T. Sato, and S. Kawakami, "Superprism phenomena in photonic crystals," *Phys. Rev. B*, vol. 58, pp. R10096–R10099, 1998.

[12] ——, "Self-collimating phenomena in photonic crystals," *Appl. Phys. Lett.*, vol. 74, pp. 1212–1214, 1999.

[13] S. Kawakami, "Fabrication of submicrometre 3D periodic structures composed of Si/SiO_2," *Electron. Lett.*, vol. 33, pp. 1260–1261, 1997.

[14] M. Notomi, "Theory of light propagation in strongly modulated photonic crystals: Refractionlike behavior in the vicinity of the photonic band gap," *Phys. Phys. Phys. Rev. B*, vol. 62, pp. 10 696–10 705, 2000.

[15] M. Lončar, J. Vučković, and A. Scherer, *Proc. PECS III Conf.*, 2001.

[16] L. Wu, M. Mazilu, T. Karle, and T. F. Krauss, "Superprism phenomena in planar photonic crystals," *IEEE J. Quantum Electron.*, vol. 38, pp. 915–918, 2002.

[17] T. Baba and M. Nakamura, "Photonic crystal light deflection devices using the superprism effect," *IEEE J. Quantum Electron.*, vol. 38, pp. 909–914, 2002.

[18] A. Taflove, *Computational Electrodynamics – The Finite-Difference Time-Domain Method*. Norwood, MA: Artech House, 1995.

[19] M. Lončar, D. Nedeljkovic, and T. P. Pearsall *et al.*, "Experimental and theoretical confirmation of Bloch-mode light propagation in planar photonic crystal waveguides," *Appl. Phys. Lett.*, vol. 80, pp. 1689–1691, 2002.

[20] Y. Désières *et al.*, "Propagation losses of the fundamental mode in a single line-defect photonic crystal waveguide on an InP membrane," *J. Appl. Phys.*, vol. 92, pp. 2227–2234, 2002.

Jeremy Witzens was born in Strasbourg, France, in 1978. He received the Diploma in engineering from the Ecole Polytechnique, France, in 2000 and the M.S. degree in electrical engineering from the California Institute of Technology (Caltech), Pasadena, in 2001. He is currently working toward the Ph.D. degree at Caltech.

His research interests include design and fabrication of integrated optics devices, dispersion properties of photonic crystals, and nonlinear phenomena in photonic crystals.

Marko Lončar was born in Dubrovnik, Croatia, in 1974. He received the Diploma in engineering from the University of Belgrade, Yugoslavia, in 1997 amd the M.S. degree in electrical engineering from California Institute of Technology (Caltech), Pasadena, in 1998. He is currently working toward the Ph.D. degree in electrical engineering at Caltech.

His research interests include design and fabrication of nanooptic devices and ultrasmall device processing techniques.

Axel Scherer received the B.S., M.S., and Ph.D. degrees from the New Mexico Institute of Mining and Technology in 1981, 1982, and 1985, respectively.

From 1985 until 1993, he worked in the Quantum Device Fabrication Group at Bellcore. Currently, he is the Bernard E. Neches Professor of Electrical Engineering, Applied Physics, and Physics at the California Institute of Technology, Pasadena, specializing in device microfabrication. His research interests include design and fabrication of functional photonic, nanomagnetic, and microfluidic devices.